E. A. Codling · N. A. Hill

Calculating spatial statistics for velocity jump processes with experimentally observed reorientation parameters

Abstract. Mathematical modelling of the directed movement of animals, microorganisms and cells is of great relevance in the fields of biology and medicine. Simple diffusive models of movement assume a random walk in the position, while more realistic models include the direction of movement by assuming a random walk in the velocity. These velocity jump processes, although more realistic, are much harder to analyse and an equation that describes the underlying spatial distribution only exists in one dimension. In this communication we set up a realistic reorientation model in two dimensions, where the mean turning angle is dependent on the previous direction of movement and bias is implicitly introduced in the probability distribution for the direction of movement. This model, and the associated reorientation parameters, is based on data from experiments on swimming microorganisms. Assuming a transport equation to describe the motion of a population of random walkers using a velocity jump process, together with this realistic reorientation model, we use a moment closure method to derive and solve a system of equations for the spatial statistics. These asymptotic equations are a very good match to simulated random walks for realistic parameter values.

1. Introduction

Individual based diffusion models that use an uncorrelated random walk in the spatial position are known as *position jump processes* (Othmer et al., 1988). These simple models do not include directional effects in the movement and are only valid as long-time approximations to the behaviour of the population as they allow for effectively infinite propagation speeds (Okubo, 1980; Othmer et al., 1988). A more realistic approach is to use a

E. A. Codling: Department of Applied Mathematics, University of Leeds, Leeds, LS2 9JT, UK. e-mail: `eddc@maths.leeds.ac.uk`

N. A. Hill: Department of Mathematics, University of Glasgow, Glasgow, G12 8QQ, UK. e-mail: `n.a.hill@maths.gla.ac.uk`

E.A.C. address now: Department of Zoology, Ecology and Plant Science, University College Cork, Cork, Ireland.

Correspondence to: N. A. Hill

random walk in the velocity known as a *velocity jump process* (Othmer et al., 1988; Hillen & Othmer, 2000; Othmer & Hillen, 2002). These models result in a correlated random walk in space and directional effects can be included. As a fixed or bounded speed can be assumed, they also avoid the problem of infinte propagation that is found in diffusive models based on position jump processes (Okubo, 1980; Othmer et al., 1988).

In one dimension, the simplest form of the velocity jump process is the well known Goldstein–Kac equation or *telegraph equation* (Goldstein, 1953; Kac, 1974). However, in two dimensions there is no closed form equation for the underlying spatial distribution (Hillen, 2002). It is possible to use a linear transport equation that describes the velocity jump process to derive differential equations for the moments of the underlying spatial distribution. However, the resulting system of differential equations is only closed in particular special cases (Othmer et al., 1988; Hillen, 2002). In general, it is necessary to make some assumption or approximation about the higher order moments in order to close and solve the system.

When considering the case of a random walk in an external field, Othmer et al. (1988) use a velocity jump process with a fixed speed where the new angular direction of movement is only dependent on the current direction of movement. For a special case, they derive a closed system of differential equations for the spatial statistics by assuming that the reorientation kernel, $T(\theta, \theta')$, is a superposition of two separate probability distributions that take into account the correlation and the bias effects separately (see Othmer et al. (1988) Sec. 4.2 and Fig. 4).

Although there has been much recent discussion comparing the suitability of the velocity jump and position jump processes to various models of movement (see for example Othmer et al., 1988; Ford & Lauffenburger, 1991; Dolak & Hillen, 2003), we are not aiming to compare the two processes directly. Rather, we exploit the fact that the velocity jump process allows for the direction of movement of the individual walkers to be explicitly modelled. In our case, movement is modelled using a realistic individual-based reorientation model that implicitly includes bias effects and has parameters that have been observed experimentally (Hill & Häder, 1997). We derive a closed system of differential equations by making several assumptions about the parameter values and the higher order moments, and compare solutions to simulations of random walks that use this reorientation model.

2. Transport equation

In a similar manner to Othmer et al. (1988) (see also Hillen & Othmer, 2000; Othmer & Hillen, 2002), we use a transport equation to describe the velocity jump process used by our walkers. We assume that the turning frequency is given by a Poisson process of intensity λ, so that the time between turns has an Exponential distribution with mean $\bar{\tau} = 1/\lambda$.

Suppose we have an infinite two-dimensional phase space, $\mathbf{x} = (x_1, x_2)$ with a preferred direction along the positive x_1-axis of the plane, under

the assumption that the bias only influences the turning angle distribution $T(\theta, \theta')$. We have a population of individuals, p, moving with constant speed, s, and turning with average time between turns, $\bar{\tau}$. The appropriate density function is $p(\mathbf{x}, \theta, t)$ where θ is the angle between the current direction of motion and the positive x_1-axis. The direction of travel is $\boldsymbol{\xi} = (\cos\theta, \sin\theta)$ and the preferred direction is $\boldsymbol{\xi}_1 = (1, 0)$. The transport equation is (Othmer et al., 1988)

$$\frac{\partial p}{\partial t} + s\boldsymbol{\xi}.\nabla_{\mathbf{x}} p = -\lambda p + \lambda \int_{-\pi}^{\pi} T(\theta, \theta') \, p(\mathbf{x}, \theta', t) \, d\theta'. \tag{1}$$

In (1) the random changes of direction are introduced through the reorientation kernel $T(\theta, \theta')$. The total population remains fixed and is given by

$$\int_{R^2} \int_{-\pi}^{\pi} p(\mathbf{x}, \theta, t) \, d\theta \, d\mathbf{x} = N_0. \tag{2}$$

As the domain is infinite and the speed of movement is bounded, we assume that as $\mathbf{x} \to \infty$, $p(\mathbf{x}, \theta, t) \to 0$ and any boundary terms vanish at infinity, see Othmer et al. (1988), p. 280 and Codling (2003).

The reorientation kernel, $T(\theta, \theta')$, used in our velocity jump process is described in the next section.

3. Reorientation kernel

The simplest random walk models are fixed on a square lattice, and in two dimensions there is only a choice of four possible directions of movement. A more realistic model is not restricted to a lattice and allows for movement in any direction at each step. This requires a probability distribution function (p.d.f.) for the turning angle, δ.

Probability distribution functions on a circle, $f(\theta)$, satisfy

$$f(\theta) \geq 0 \ \ \forall \ -\pi \leq \theta < \pi, \tag{3}$$

and the normalization condition that

$$\int_{-\pi}^{\pi} f(\theta) \, d\theta = 1. \tag{4}$$

The simplest unimodal circular distributions to use for the p.d.f. of the turning angle are the wrapped normal and von Mises distributions (Batschelet, 1981; Mardia & Jupp, 1999). Both distributions have a similar shape and, as they differ by only a few percent for appropriate choices of parameters, they are often assumed to be equivalent. The mean of both distributions is given by μ_δ, while the spread is measured differently. The wrapped normal has an angular variance, σ_δ^2, analogous to the variance of the linear normal distribution; whereas the von Mises distribution has a *concentration parameter*, κ. A relation between these two parameters can

be found by equating the first moments (mean resultant lengths) of the distributions, see Sec. 3.2.

The von Mises and wrapped normal distributions have been used as the p.d.f. for the turning angle, δ, to model *correlated* and *unbiased* random walks (e.g. Siniff & Jessen, 1969; Kareiva & Shigesada, 1983; Bovet & Benhamou, 1988). In these models the mean turning angle, μ_δ, is assumed to be zero so that there is a tendency to continue moving in the same direction — a realistic model for animal motion where there is no overall preferred direction of movement. If the mean turning angle, μ_δ, is made dependent on the absolute angle, θ, then *bias* can be introduced into the turning angle distribution as we shall show below. This is in contrast to the example considered by Othmer et al. (1988) who used a superposition of two separate probability distributions for correlation and bias in their random walk in an external field, see Sec. 4.2 and Fig. 4 in Othmer et al. (1988).

3.1. The von Mises distribution

Henceforth we define θ' to be the previous direction of movement, and θ as the new direction of movement after reorientation, so that the turning angle is given by $\delta = \theta - \theta'$ (where $-\pi \leq \delta < \pi$).

For our reorientation kernel, $T(\theta, \theta')$, we use the von Mises distribution which is easier to work with analytically than the wrapped normal distribution. This is defined by

$$T(\theta, \theta') = \frac{1}{2\pi I_0(\kappa)} \, \exp\left(\kappa \cos(\delta - \mu_\delta)\right), \tag{5}$$

where I_n denotes the modified Bessel function of the first kind and order n, which is defined by

$$I_n(\kappa) = \frac{1}{2\pi} \int_{-\pi}^{\pi} \cos n\theta \exp\left(\kappa \cos \theta\right) d\theta. \tag{6}$$

When $\kappa = 0$ the von Mises distribution equals the uniform distribution, and as $\kappa \to \infty$ the distribution becomes sharply peaked about the mean turning angle μ_δ (Batschelet, 1981; Mardia & Jupp, 1999). For the von Mises distribution, the n-th moment is given by $\rho_n = A_n(\kappa)$ (Mardia & Jupp, 1999) where

$$A_n(\kappa) = I_n(\kappa)/I_0(\kappa). \tag{7}$$

Note that because of the dependence of $\mu_\delta(\theta')$ on θ' introduced in Sec. 4.1, our reorientation kernel violates assumption T4 made by Hillen & Othmer (2000) and Hillen (2002) in their general theory of velocity jump processes. That is, a simple calculation shows that in general

$$\int_{-\pi}^{\pi} T(\theta, \theta') \, d\theta' \neq 1, \tag{8}$$

for our velocity jump process, although the usual normalisation condition

$$\int_{-\pi}^{\pi} T(\theta, \theta') \, d\theta = 1, \tag{9}$$

does hold (condition T1 in Hillen & Othmer (2000)).

3.2. Relation between the wrapped normal and von Mises distributions

If the first moments, ρ_1, of the wrapped normal and von Mises distributions are equal then the relation between σ_δ and κ is given by

$$\rho_1 = A_1(\kappa) = \exp\left(-\sigma_\delta^2/2\right), \tag{10}$$

and the two distributions only differ by a few percent so that in applications it is convenient to treat their properties as being the same (Mardia & Jupp, 1999). The function $A_1(\kappa)$ and its inverse $A^{-1}(\kappa)$ are readily computed numerically, or can be found by looking at tables of the inverse Bessel functions (Batschelet, 1981; Mardia & Jupp, 1999). Assuming (10) holds then, as $\kappa \to 0$, $\sigma_\delta^2 \to \infty$ asymptotically; and as $\kappa \to \infty$, $\sigma_\delta^2 \to 0$ asymptotically.

In the next section, we describe how we use the results from Hill & Häder (1997) to give a range of values for κ, and a functional form for μ_δ that introduces bias, both used in our velocity jump process.

4. The random walk on a circle as a model for the reorientation of swimming microorganisms

Hill & Häder (1997) carried out experiments to observe and analyse the trajectories of swimming microorganisms such as the alga *Chlamydomonas nivalis*. By calculating the angular statistics of the trajectories and comparing to a theoretical random walk on a unit circle, they were able to estimate parameters such as the mean reorientation time, B, and the unit angular variance, σ_0^2. *C. nivalis* is known to be influenced by both *gyrotaxis* due to the balance between gravitational and viscous torques, as the algae are bottom heavy (Kessler, 1986), and *phototaxis* as the algae are sensitive to light (Hill & Vincent, 1993; Ghovai & Hill, 2004).

4.1. The Fokker–Planck equation and reorientation models

Hill & Häder (1997) set up a simple random walk in the absolute angle of movement, θ, as a position jump process on a unit circle. Consistent with standard random walk theory, they assumed that the mean turning angle, μ_δ, and the variance of the turning angle, σ_δ^2 are proportional to the time step between turns, τ, in the limit as $\tau \to 0$, i.e.

$$\mu_\delta(\theta, \tau) = \mu_0(\theta)\tau, \tag{11}$$
$$\sigma_\delta^2(\theta, \tau) = \sigma_0^2(\theta)\tau. \tag{12}$$

In this limit the Fokker–Planck equation for the probability density function of the absolute angle, $f(\theta, t)$, is

$$\frac{\partial}{\partial t} f(\theta, t) = -\frac{\partial}{\partial \theta} [\mu_0(\theta) f(\theta, t)] + \frac{1}{2} \frac{\partial^2}{\partial \theta^2} [\sigma_0^2(\theta) f(\theta, t)]. \qquad (13)$$

Based on their experimental data, Hill & Häder (1997) suggested the following forms for the mean turning angle, μ_δ:

$$\mu_\delta(\theta, \tau) = -d_\tau \sin \theta, \quad -\pi \le \theta < \pi, \qquad (14)$$

for *sinusoidal* reorientation corresponding to gyrotaxis, and

$$\mu_\delta(\theta, \tau) = \begin{cases} -d_\tau \theta, & -\pi < \theta < \pi, \\ 0, & \theta = \pm\pi, \end{cases} \qquad (15)$$

for *linear* reorientation corresponding to phototaxis, where $d_\tau = \tau/B$ is a dimensionless parameter and, without loss of generality, the preferred direction is assumed to be $\theta = 0$. The fact that the mean turning angle, μ_δ, is dependent on the previous direction of movement, θ, introduces *bias* into the motion. Hill & Häder (1997) assumed that σ_0^2 is constant and independent of the absolute angle, θ.

4.2. Steady state solutions of the Fokker–Planck equation

For sinusoidal reorientation, where μ_δ is as defined in (14), the normalized solution of the *steady state* Fokker–Planck equation (13), plus appropriate boundary conditions, is the von Mises distribution:

$$f(\theta) = M(\theta; \theta_0, 2z) = \frac{1}{2\pi I_0(2z)} \exp\left(2z \cos(\theta - \theta_0)\right), \qquad (16)$$

where $z = (B\sigma_0^2)^{-1}$.

For linear reorientation, where μ_δ is as defined in (15), the normalized solution of the steady state Fokker–Planck equation (13), plus appropriate boundary conditions, can be shown to be

$$f(\theta) = N(z) \exp\left(-z\theta^2\right), \qquad (17)$$

where $z = (B\sigma_0^2)^{-1}$ and $N(z)$ is the normalization function defined by

$$N(z) = \left(\int_{-\pi}^{\pi} \exp\left(-z\theta^2\right) \, d\theta\right)^{-1} = \sqrt{z} \left(\sqrt{\pi} \, \mathrm{erf}(\pi\sqrt{z})\right)^{-1}. \qquad (18)$$

Thus, (16) and (17) give the expected long-time (steady-state) probability distributions for the absolute angle, θ.

Table 1. Parameter values observed by Hill & Häder (1997) in experiments on the swimming algae *C. nivalis*. Data set C1 corresponds to algae moving with gyrotaxis which is modelled using a sinusoidal reorientation model; data set C4 corresponds to algae moving with phototaxis which is modelled using a linear reorientation model. Values in brackets are estimates calculated using only the smaller sampling time steps, $\tau_s < 0.4$ s. We refer to parameter values calculated using all sampling time steps as data sets C1:a and C4:a, while those parameter values calculated using only the smaller sampling time steps, $\tau_s < 0.4$ s, are referred to as C1:b and C4:b. In our velocity jump process we assume $\bar{\tau} = 0.08$ s, while κ has been calculated from σ_δ^2 using (10).

Data	B^{-1}	σ_0	$d_\tau = B^{-1}\bar{\tau}$	$\sigma_\delta^2 = \sigma_0^2\bar{\tau}$	κ
C1:a(b)	0.37 (0.80)	1.3 (2.0)	0.030 (0.064)	0.136 (0.320)	7.89 (3.73)
C4:a(b)	0.19 (0.61)	0.9 (1.7)	0.015 (0.050)	0.064 (0.224)	16.14 (5.03)

4.3. Using the reorientation models in a velocity jump process

By rediscretizing the trajectories of swimming microorganisms with different fixed sampling time steps, τ_s, observing μ_δ and σ_δ^2 for each time step, and assuming the linear dependence given in (11) and (12), Hill & Häder (1997) were able to estimate the parameters B^{-1} and σ_0, see Table 1. Data set C1 corresponds to *C. nivalis* moving in a vertical plane subject to gyrotaxis, while C4 corresponds to *C. nivalis* moving in a horizontal plane and exhibiting phototaxis due to a fixed light source. As Hill & Häder (1997) were unsure as to the point at which the sampling time step, τ_s, becomes too large and the linear relations in (11) and (12) break down, they made two estimates for each parameter by using either all time steps, or only the smaller time steps, $\tau_s < 0.4$ s. In Codling & Hill (2004), we show that the estimates using only $\tau_s < 0.4$ s are likely to be much closer to the true values of the reorientation parameters.

Hill & Häder (1997) assumed that the underlying random walk was 'smooth' in the sense that the walkers were continuously turning. A velocity jump process is made up of discrete steps of fixed length and is clearly not smooth. However, if the average time step between turns, $\bar{\tau} \to 0$, the velocity jump process becomes 'approximately smooth', and from (11) and (12), μ_δ, $\sigma_\delta^2 \to 0$. In the following analysis we make the assumption that our velocity jump process is smooth, and assume that d_τ and $\bar{\tau}$ are both small. Table 1 gives values for d_τ and κ calculated from the data of Hill & Häder (1997), assuming that $\bar{\tau} = 0.08$ s (the smallest sampling time step used by Hill & Häder (1997) due to experimental constraints).

5. The spatial moments

We are interested in the mean location of the population of walkers, $\mathbf{H}(t)$, their mean velocity, $\mathbf{V}(t)$, their mean squared displacement, $D^2(t)$, and their mean squared deviation, $\sigma^2(t)$, which is a measure of the fluctuations of the

individual's path around the expected path. The definitions are

$$\mathbf{H}(t) = \frac{1}{N_0} \int_{R^2} \int_{-\pi}^{\pi} \mathbf{x} \, p(\mathbf{x}, \theta, t) \, d\theta \, d\mathbf{x}, \tag{19}$$

$$\mathbf{V}(t) = \frac{s}{N_0} \int_{R^2} \int_{-\pi}^{\pi} \boldsymbol{\xi} \, p(\mathbf{x}, \theta, t) \, d\theta \, d\mathbf{x}, \tag{20}$$

$$\text{and} \quad D^2(t) = \frac{1}{N_0} \int_{R^2} \int_{-\pi}^{\pi} \|\mathbf{x}\|^2 \, p(\mathbf{x}, \theta, t) \, d\theta \, d\mathbf{x}, \tag{21}$$

while the mean squared deviation can be defined in terms of the other statistics as

$$\sigma^2(t) = \frac{1}{N_0} \int_{R^2} \int_{-\pi}^{\pi} \|\mathbf{x} - \mathbf{H}(t)\|^2 \, p(\mathbf{x}, \theta, t) \, d\theta \, d\mathbf{x} = D^2(t) - \|\mathbf{H}(t)\|^2. \tag{22}$$

We also define the following:

$$D_1^2(t) = \frac{1}{N_0} \int_{R^2} \int_{-\pi}^{\pi} x_1^2 \, p(\mathbf{x}, \theta, t) \, d\theta \, d\mathbf{x}, \tag{23}$$

$$D_2^2(t) = \frac{1}{N_0} \int_{R^2} \int_{-\pi}^{\pi} x_2^2 \, p(\mathbf{x}, \theta, t) \, d\theta \, d\mathbf{x}, \tag{24}$$

and

$$\sigma_1^2(t) = D_1^2(t) - \|\mathbf{H}_1(t)\|^2, \tag{25}$$
$$\sigma_2^2(t) = D_2^2(t) - \|\mathbf{H}_2(t)\|^2. \tag{26}$$

We assume that at $t = 0$ the population of walkers all start at the origin, $(0, 0)$, with a uniform distribution of initial directions. Hence, all the statistics defined in (19)-(26) are zero at $t = 0$.

6. Calculating the spatial statistics for the sinusoidal reorientation model

Using the transport equation, (1), and the reorientation kernel, (5), together with the sinusoidal reorientation model, (14), we now complete a moment-closure method to derive and solve differential equations for the statistics of the underlying spatial distribution.

6.1. Higher order moments

In a similar manner to Sect. 5 we define the following higher order moments required subsequently:

$$F_n(t) = \frac{1}{N_0} \int_{R^2} \int_{-\pi}^{\pi} \cos n\theta \, p(\mathbf{x}, \theta, t) \, d\theta \, d\mathbf{x}, \tag{27}$$

$$G_n(t) = \frac{1}{N_0} \int_{R^2} \int_{-\pi}^{\pi} x_1 \cos n\theta \, p(\mathbf{x}, \theta, t) \, d\theta \, d\mathbf{x}, \tag{28}$$

$$Y_n(t) = \frac{1}{N_0} \int_{R^2} \int_{-\pi}^{\pi} \sin n\theta \; p(\mathbf{x}, \theta, t) \; d\theta \; d\mathbf{x}, \tag{29}$$

$$\text{and} \quad Z_n(t) = \frac{1}{N_0} \int_{R^2} \int_{-\pi}^{\pi} x_2 \sin n\theta \; p(\mathbf{x}, \theta, t) \; d\theta \; d\mathbf{x}, \tag{30}$$

where $n = 1, 2, 3, \cdots$. Using these definitions, $\mathbf{V}(t) = s(F_1(t), Y_1(t))$. When the initial position is $(0,0)$ and there is a uniform distribution of initial directions, then the higher moments (27)-(30) are all zero at $t = 0$.

6.2. Closure assumptions

Closure assumption 1

From standard integrals of the von Mises distribution (Mardia & Jupp, 1999) we can derive the following integrals

$$\int_{-\pi}^{\pi} \frac{\cos n\theta}{2\pi I_0(\kappa)} \; e^{\kappa \cos(\theta - \theta' + d_\tau \sin \theta')} d\theta = \frac{I_n(\kappa)}{I_0(\kappa)} \cos(n\theta' - nd_\tau \sin \theta'), \tag{31}$$

$$\int_{-\pi}^{\pi} \frac{\sin n\theta}{2\pi I_0(\kappa)} \; e^{\kappa \cos(\theta - \theta' + d_\tau \sin \theta')} d\theta = \frac{I_n(\kappa)}{I_0(\kappa)} \sin(n\theta' - nd_\tau \sin \theta'), \tag{32}$$

which occur during the derivation of the moment equations. To make further analytic progress, we assume that the average time between turning events is small, $\bar{\tau} \ll 1$, and recall the definition, $d_\tau = B^{-1}\tau$. From the experimentally observed values of B^{-1} in Table 1, $0 \le d_\tau \ll 1$, and we seek an asymptotic expansion in powers of d_τ for the trigonometric functions. The trigonometric terms are expanded as Taylor series

$$\cos(n\theta - nd_\tau \sin \theta) = \cos n\theta + nd_\tau \sin \theta \sin n\theta - \frac{n^2 d_\tau^2}{2} \sin^2 \theta \cos n\theta, \tag{33}$$

$$\sin(n\theta - nd_\tau \sin \theta) = \sin n\theta - nd_\tau \sin \theta \cos n\theta - \frac{n^2 d_\tau^2}{2} \sin^2 \theta \sin n\theta, \tag{34}$$

correct to $O(d_\tau^3)$. Using standard trigonometric identities, (33) and (34) reduce for $n = 1$ and $n = 2$ to

$$\cos(\theta - d_\tau \sin \theta) = \frac{d_\tau}{2} + \left(1 - \frac{d_\tau^2}{8}\right) \cos \theta - \frac{d_\tau}{2} \cos 2\theta + \frac{d_\tau^2}{8} \cos 3\theta, \tag{35}$$

$$\cos(2\theta - 2d_\tau \sin \theta) = \frac{d_\tau^2}{2} + d_\tau \cos \theta + \left(1 - d_\tau^2\right) \cos 2\theta - d_\tau \cos 3\theta, \tag{36}$$

$$\sin(\theta - d_\tau \sin \theta) = \left(1 - \frac{3d_\tau^2}{8}\right) \sin \theta - \frac{d_\tau}{2} \sin 2\theta + \frac{d_\tau^2}{8} \sin 3\theta, \tag{37}$$

$$\sin(2\theta - 2d_\tau \sin \theta) = d_\tau \sin \theta + \left(1 - d_\tau^2\right) \sin 2\theta - d_\tau \sin 3\theta. \tag{38}$$

Closure assumption 2

To close the system of derived differential equations we make an assumption about the form of the underlying spatial distribution $p(\mathbf{x}, \theta, t)$. In general, it is not the case that the $\mathbf{x}$ and θ components of $p(\mathbf{x}, \theta, t)$ are independent. However, for several of the higher moments in the system we assume that when averaging over all positions $\mathbf{x}$, we can approximate $p(\mathbf{x}, \theta, t)$ by

$$p(\mathbf{x}, \theta, t) = f(\theta)p^*(\mathbf{x}, t), \tag{39}$$

where $f(\theta)$ is the long-time angular distribution given by (16), and

$$\int_{-\pi}^{\pi} f(\theta) \, d\theta = 1 \qquad \text{and} \qquad \frac{1}{N_0} \int_{R^2} p^*(\mathbf{x}, t) \, d\mathbf{x} = 1. \tag{40}$$

Under this assumption, and using the standard integrals of the von Mises distribution (Mardia & Jupp, 1999) we get

$$F_n(t) = \frac{I_n(2z)}{I_0(2z)} \equiv A_n(2z), \tag{41}$$

$$G_n(t) = \frac{I_n(2z)}{I_0(2z)} \bar{x}_1 = A_n(2z)\bar{x}_1(t), \tag{42}$$

$$Y_n(t) = 0, \tag{43}$$

$$Z_n(t) = 0, \tag{44}$$

where $z = (B\sigma_0^2)^{-1}$, and $\bar{x}_1 = \mathbf{H}(t).\boldsymbol{\xi}_1$. Note that (41) is independent of t, while (42) is dependent on t. These approximations are shown to be a good match to large time numerical simulations for all n if the assumption that $\bar{\tau}$ is small holds (Codling, 2003). In (33) and (34), terms of $O(d_\tau^m)$ for $m \geq 3$ are truncated, and to be consistent we use (41) and (42) for $n \geq 3$ also. The choice to approximate $F_n(t)$ and $G_n(t)$ for $n \geq 3$ is justified as the following analysis shows that these higher order terms are multiplied by small coefficients and are not significant. If this approximation is made for $n < 3$ then the final solutions are not valid for all time and do not match well with numerical simulations.

6.3. *Deriving differential equations for the moments*

To illustrate how to derive the differential equations for the statistics and higher order moments of the underlying spatial distribution we give the example of calculating the equation for the moment $F_1(t)$ as defined by (27).

Multiply the linear transport equation (1) by $\cos\theta$, integrate over θ and $\mathbf{x}$, and divide by N_0, to give

$$\frac{1}{N_0} \int_{R^2} \int_{-\pi}^{\pi} \cos\theta \, \frac{\partial p}{\partial t} \, d\theta \, d\mathbf{x} = -\frac{s}{N_0} \int_{R^2} \int_{-\pi}^{\pi} \cos\theta \, (\boldsymbol{\xi}.\nabla_{\mathbf{x}} p) \, d\theta \, d\mathbf{x}$$

$$-\frac{\lambda}{N_0} \int_{R^2} \int_{-\pi}^{\pi} \cos\theta \, p \, d\theta \, d\mathbf{x} + \frac{\lambda}{N_0} \int_{R^2} \int_{-\pi}^{\pi} \int_{-\pi}^{\pi} \cos\theta \, T(\theta, \theta')p(\theta')d\theta' d\theta \, d\mathbf{x}.$$

Using the definitions for $F_n(t)$ from (27)and for $T(\theta, \theta')$ from (5) together with the sinusoidal reorientation model, (14), gives

$$
\frac{dF_1}{dt} = -\frac{s}{N_0} \int_{R^2} \int_{-\pi}^{\pi} \nabla_{\mathbf{x}}.(\cos\theta \boldsymbol{\xi} p) \ d\theta \ d\mathbf{x} - \lambda F_1
$$
$$
+ \frac{\lambda}{N_0} \int_{R^2} \int_{-\pi}^{\pi} \int_{-\pi}^{\pi} \frac{\cos\theta}{2\pi I_0(\kappa)} \ e^{\kappa\cos(\theta-\theta'+d_\tau\sin\theta)} \ p(\theta') \ d\theta' \ d\theta \ d\mathbf{x}.
$$

As we assume the probability density and associated boundary terms are zero at infinity, use of the divergence theorem shows that the first term in the right hand side of the above is zero, see Codling (2003) for full details. The order of the integration in the third term can be changed, and using the von Mises integral (31), we get

$$
\frac{dF_1}{dt} = -\lambda F_1 + \frac{\lambda I_1(\kappa)}{N_0 I_0(\kappa)} \int_{R^2} \int_{-\pi}^{\pi} \cos(\theta' - d_\tau \sin\theta') \ p(\theta') \ d\theta' \ d\mathbf{x}.
$$

Using closure assumptions 1 and 2 and expanding using (35) gives

$$
\frac{dF_1}{dt} = -\lambda_{11} F_1 + \hat{a}_1 - \hat{a}_1 F_2 + \hat{a}_2 A_3(2z), \tag{45}
$$

which is correct to $O(d_\tau^3)$. The constant terms are given by

$$
\lambda_{11} = \lambda\left(1 - (1 - \frac{d_\tau^2}{8})A_1(\kappa)\right), \quad \hat{a}_1 = \frac{\lambda d_\tau A_1(\kappa)}{2}, \quad \hat{a}_2 = \frac{\lambda d_\tau^2 A_1(\kappa)}{8}. \tag{46}
$$

6.4. Final system of differential equations and solutions

Using the same method as in Sect. 6.3 we derive the leading order system of differential equations for the higher moments of the spatial distribution as given in Appendix A.1. The system is only an approximation as higher order terms have been omitted using the closure assumptions given in Sect. 6.2.

Solving the system of linear differential equations is straightforward (Codling, 2003). The solution for $\mathbf{V}(t)$ is

$$
\mathbf{V}(t) = s\left(A_{f1}\left(1 - e^{-\phi_1 t}\right) + B_{f1}\left(1 - e^{-\phi_2 t}\right)\right)\boldsymbol{\xi}_1, \tag{47}
$$

and the solution for $\mathbf{H}(t)$ is

$$
\mathbf{H}(t) = s\left((A_{f1} + B_{f1})t - \frac{A_{f1}}{\phi_1}\left(1 - e^{-\phi_1 t}\right) - \frac{B_{f1}}{\phi 2}\left(1 - e^{-\phi_2 t}\right)\right)\boldsymbol{\xi}_1, \tag{48}
$$

where the coefficients in the solutions are defined in Appendix A.3.

The solutions for the spread about the origin in each direction are

$$
D_1^2(t) = A_{D1} + B_{D1}t + C_{D1}t^2 + E_{D1}(t), \tag{49}
$$
$$
D_2^2(t) = A_{D2} + B_{D2}t + E_{D2}(t), \tag{50}
$$

where A_{D1}, B_{D1}, etc are constants, and E_{D1} and E_{D2} are decaying exponential terms. The full solutions for $D_1^2(t)$ and $D_2^2(t)$ are given in (90) and (91) in Appendix A.2. The total spread about the origin is given by

$$D^2(t) = D_1^2(t) + D_2^2(t), \tag{51}$$

which is calculated from (49) and (50). Using these solutions for $\mathbf{H}(t)$, $D_1^2(t)$ and $D_2^2(t)$, the spread about the mean position in each direction, $\sigma_1^2(t)$ and $\sigma_2^2(t)$, can be calculated from (25) and (26) but we omit the full solutions given in Codling (2003).

It is interesting to note that $D_2^2(t) \propto t$, the usual behaviour for a diffusive process, but $D_1^2(t) \propto t^2$. This is explained by the fact that, in a biased random walk, there is always an average drift in the preferred direction (given by $\mathbf{H}(t) \propto t$ in our walk). Thus, the spread about the origin in the preferred direction, $D_1^2(t)$, will be dominated by this average drift term. If we consider the spread about the *mean position*, or if the random walk is unbiased, then this average drift is not included, $\sigma_1^2(t) \propto t$ and $\sigma_2^2(t) \propto t$, and the spread is purely diffusive.

If $d_\tau = 0$ and there is no bias in the system, then the original differential equations for $G_1(t)$ and $Z_1(t)$, (86) and (87) given in Appendix A.1, reduce to

$$\frac{dG_1}{dt} = \frac{s}{2} - \lambda_0 G_1, \tag{52}$$

$$\frac{dZ_1}{dt} = \frac{s}{2} - \lambda_0 Z_1, \tag{53}$$

where $\lambda_0 = \lambda \left(1 - I_1(\kappa)/I_0(\kappa)\right)$. This gives the solution

$$D_1^2(t) = D_2^2(t) = \frac{s^2}{\lambda_0} \left(t - \frac{1}{\lambda_0}(1 - e^{-\lambda_0 t}) \right), \tag{54}$$

and the spread about the origin is the same in each direction. Thus, if there is no bias in the random walk, our equation for the total spread about the origin, (51), is the same as that derived by Othmer et al. (1988) for their random walk with no bias (equations (49) and (50) in their paper). Note also that in the case of zero bias, there is no average drift and the mean position is the origin. Hence in this case $D_1^2(t) = D_2^2(t) = \sigma_1^2(t) = \sigma_2^2(t)$.

7. Calculating the spatial statistics for the linear reorientation model

Using the transport equation, (1), and the reorientation kernel, (5), together with the linear reorientation model, (15), we now complete a moment-closure method to derive and solve differential equations for the statistics of the underlying spatial distribution in a similar way to Sect. 6.

7.1. Higher order moments

In a similar manner to Sect. 5 we define the following higher order moments which are required when deriving the differential equations for the statistics of interest:

$$K_n(t) = \frac{1}{N_0} \int_{R^2} \int_{-\pi}^{\pi} \theta \sin n\theta \ p(\mathbf{x}, \theta, t) \ d\theta \ d\mathbf{x}, \tag{55}$$

$$L_n(t) = \frac{1}{N_0} \int_{R^2} \int_{-\pi}^{\pi} \theta \cos n\theta \ p(\mathbf{x}, \theta, t) \ d\theta \ d\mathbf{x}, \tag{56}$$

$$M_n(t) = \frac{1}{N_0} \int_{R^2} \int_{-\pi}^{\pi} \theta^2 \cos n\theta \ p(\mathbf{x}, \theta, t) \ d\theta \ d\mathbf{x}, \tag{57}$$

$$N_n(t) = \frac{1}{N_0} \int_{R^2} \int_{-\pi}^{\pi} \theta^2 \sin n\theta \ p(\mathbf{x}, \theta, t) \ d\theta \ d\mathbf{x}, \tag{58}$$

$$P_n(t) = \frac{1}{N_0} \int_{R^2} \int_{-\pi}^{\pi} x_1 \theta \sin n\theta \ p(\mathbf{x}, \theta, t) \ d\theta \ d\mathbf{x}, \tag{59}$$

$$Q_n(t) = \frac{1}{N_0} \int_{R^2} \int_{-\pi}^{\pi} x_2 \theta \cos n\theta \ p(\mathbf{x}, \theta, t) \ d\theta \ d\mathbf{x}, \tag{60}$$

$$R_n(t) = \frac{1}{N_0} \int_{R^2} \int_{-\pi}^{\pi} x_1 \theta^2 \cos n\theta \ p(\mathbf{x}, \theta, t) \ d\theta \ d\mathbf{x}, \tag{61}$$

$$\text{and} \ \ S_n(t) = \frac{1}{N_0} \int_{R^2} \int_{-\pi}^{\pi} x_2 \theta^2 \sin n\theta \ p(\mathbf{x}, \theta, t) \ d\theta \ d\mathbf{x}, \tag{62}$$

for $n = 1, 2, 3, \cdots$. The higher moments $F_n(t)$, $G_n(t)$, $Y_n(t)$ and $Z_n(t)$, defined in (27)-(30), are also required. Assuming all walkers start at the origin with a uniform distribution of directions at $t = 0$, the initial conditions are $F_n(0) = G_n(0) = Y_n(0) = Z_n(0) = L_n(0) = N_n(0) = 0$ and $K_1(0) = 1$, $M_1(0) = -2$, $K_2(0) = -1/2$, $M_2(0) = 1/2$.

7.2. Closure assumptions and further approximations

When using the transport equation, (1), with the linear reorientation kernel to derive a closed system of differential equations for the moments of the spatial distribution the two closure assumptions given in Sec. 6.2 are needed. Note that in closure assumption 2, the simple equations in (41) and (42) do not hold for the linear reorientation model as the steady state absolute angular distribution is different and the approximations are calculated numerically using (17).

To derive differential equations for all the higher order moments using the linear reorientation kernel it is also necessary to solve the following integrals that occur when integrating the transport equation (1):

$$k_n(\mu_\delta, \kappa) = \int_{-\pi}^{\pi} \theta \sin n\theta \ e^{\kappa \cos(\theta - \mu_\delta)} \ d\theta, \tag{63}$$

$$l_n(\mu_\delta, \kappa) = \int_{-\pi}^{\pi} \theta \cos n\theta \; e^{\kappa \cos(\theta - \mu_\delta)} \; d\theta, \tag{64}$$

$$m_n(\mu_\delta, \kappa) = \int_{-\pi}^{\pi} \theta^2 \cos n\theta \; e^{\kappa \cos(\theta - \mu_\delta)} \; d\theta , \tag{65}$$

and

$$n_n(\mu_\delta, \kappa) = \int_{-\pi}^{\pi} \theta^2 \sin n\theta \; e^{\kappa \cos(\theta - \mu_\delta)} \; d\theta , \tag{66}$$

for $n = 1$ and 2, and where $\mu_\delta = \theta' - d_\tau \theta'$. These integrals are then multiplied by $p(\mathbf{x}, \theta', t)$ and integrated over θ' and $\mathbf{x}$ to give differential equations for the moments of the population distribution.

In the absence of analytical expressions for these integrals, we fit functions of Bessel functions by inspection to solutions calculated numerically to make further progress. The fitted functions require increasingly complex terms involving higher order Bessel functions as κ increases. To avoid over-complication, the function

$$k_1(\mu_\delta, \kappa) = 2\pi I_0(\kappa) - \pi I_1(\kappa) \cos \mu_\delta - \pi I_2(\kappa), \tag{67}$$

was used to approximate (63) with $n = 1$. When $\kappa = 0$, both the exact integral and the estimate function $k_1(\mu_\delta, \kappa)$ equal 2π.

Similarly, we fitted the following functions to the integrals given in (63)-(66), for $n = 1$ and $n = 2$ respectively:

$$l_1(\mu_\delta, \kappa) = -I_1(\kappa)\pi \sin \mu_\delta + 2I_2(\kappa)\pi \sin 2\mu_\delta, \tag{68}$$

$$m_1(\mu_\delta, \kappa) = -4\pi I_0(\kappa) + 8\pi I_1(\kappa) \cos \mu_\delta - 4\pi I_2(\kappa) \cos 2\mu_\delta, \tag{69}$$

$$n_1(\mu_\delta, \kappa) = 6\pi I_1(\kappa) \sin \mu_\delta, \tag{70}$$

$$k_2(\mu_\delta, \kappa) = -\pi I_0(\kappa) + 3\pi I_1(\kappa) \cos \mu_\delta - 3/2 \; \pi I_2(\kappa) \cos 2\mu_\delta, \tag{71}$$

$$l_2(\mu_\delta, \kappa) = -3/2 \; I_1(\kappa)\pi \sin \mu_\delta - I_2(\kappa)\pi \sin 2\mu_\delta, \tag{72}$$

$$m_2(\mu_\delta, \kappa) = \pi I_0(\kappa) - 4\pi I_1(\kappa) \cos \mu_\delta + 6\pi I_2(\kappa) \cos 2\mu_\delta, \tag{73}$$

$$n_2(\mu_\delta, \kappa) = -4\pi I_1(\kappa) \sin \mu_\delta + 8\pi I_2(\kappa) \sin 2\mu_\delta. \tag{74}$$

These estimates are then used in place of the integrals (63)-(66) in order to make further analytic progress. Full details and plots of exact integrals and estimated functions are given in Codling (2003).

In general, these functions are a good fit for small values of the parameter κ but become increasingly less of a fit as κ gets larger. It should be made clear however, that if the random walk is approximately smooth and $d_\tau \ll 1$ (as we have assumed throughout), then any errors due to estimating these functions are likely to be insignificant. This is for two reasons. (i) The errors between the exact integrals and our estimated functions are greatest when μ_δ is large (Codling, 2003). However, from (15), μ_δ will always be small if $d_\tau \ll 1$. (ii) Terms involving these estimated functions are themselves multiplied by $d_\tau^n m$ terms (where $m \geq 1$) and will hence be small. In Sec. 8 our asymptotic solutions using these estimated functions are shown to fit well with simulation results. If the random walk is not approximately smooth (d_τ is large) then our asymptotic solutions are likely to be inaccurate.

7.3. Final system of differential equations and solutions

Using the same method as in Sec. 6.3 we derive the leading order system of differential equations for the higher moments of the spatial distribution as given in Appendix B.1. The system is only an approximation as higher order terms have been omitted using the closure assumptions given in Sec. 6.2. Note that the differential equations for $\mathbf{H}(t)$, $D_1^2(t)$ and $D_2^2(t)$ are the same for all reorientation kernels $T(\theta, \theta')$ (see comment at the end of Appendix A.1). Thus, these differential equations are the same for both our sinusoidal and linear reorientation models, and are the same as differential equations (74) and (76) in Othmer et al. (1988) which were derived for a different reorientation model.

To leading order, (113) in Appendix B.1 has general solutions

$$
\begin{aligned}
F_n(t) &= \tilde{A}_{fn} e^{-\phi_1 t} + \tilde{B}_{fn} e^{-\phi_2 t} + \tilde{C}_{fn}, \\
K_n(t) &= \tilde{A}_{kn} e^{-\phi_1 t} + \tilde{B}_{kn} e^{-\phi_2 t} + \tilde{C}_{kn}, \\
M_n(t) &= \tilde{A}_{mn} e^{-\phi_1 t} + \tilde{B}_{mn} e^{-\phi_2 t} + \tilde{C}_{mn},
\end{aligned} \tag{75}
$$

where $\tilde{A}_{fn}$, $\tilde{B}_{fn}$, $\tilde{C}_{fn}$ etc are all $O(1)$ constants. All the eigenvalues, ϕ_i, have negative real part, and hence any exponential terms in the solutions decay away to zero as $t \to \infty$, and the solutions tend to $O(1)$ constants.

Although the matrices in (113) and (114) are similar, the fact that all the initial conditions in (114) are zero, results in the following trivial solutions for the moments

$$
Y_n(t) = L_n(t) = N_n(t) = 0 \ \forall \ t, \tag{76}
$$

and the higher moments that correspond to the non-preferred direction are zero for all time.

The solution for $\mathbf{V}(t)$ is

$$
\mathbf{V}(t) = s \left(\tilde{A}_{f1} e^{-\phi_1 t} + \tilde{B}_{f1} e^{-\phi_2 t} + \tilde{C}_{f1} \right) \boldsymbol{\xi}_1, \tag{77}
$$

where $\tilde{A}_{f1}$, $\tilde{B}_{f1}$ and $\tilde{C}_{f1}$ are all constants such that $\tilde{C}_{f1} = -(\tilde{A}_{f1} + \tilde{B}_{f1})$ and $\mathbf{V}(0) = 0$. Note that the coefficents in the linear model are *not* the same as those defined for the sinusoidal model, $\tilde{A}_{f1} \neq A_{f1}$.

The solution for $\mathbf{H}(t)$ is

$$
\mathbf{H}(t) = s \left(\tilde{C}_{f1} t + \frac{\tilde{A}_{f1}}{\phi_1} + \frac{\tilde{B}_{f1}}{\phi_2} + \tilde{E}_H(t) \right) \boldsymbol{\xi}_1 \tag{78}
$$

where the term $\tilde{E}_H(t)$ takes into account all the decaying exponential terms dependent on the eigenvalues ϕ_i and the constants multiplying them, so that $\tilde{E}_H(t) \to 0$ as $t \to \infty$, and

$$
\mathbf{H}_\infty \sim s\tilde{C}_{f1} t \boldsymbol{\xi}_1. \tag{79}
$$

Similarly, the solutions for $D_1^2(t)$ and $D_2^2(t)$ have the form

$$D_1^2(t) = \tilde{A}_{D1} + \tilde{B}_{D1}t + \tilde{C}_{D1}t^2 + \tilde{E}_{D1}(t), \qquad (80)$$

$$D_2^2(t) = \tilde{A}_{D2} + \tilde{B}_{D2}t + \tilde{E}_{D2}(t), \qquad (81)$$

where $\tilde{A}_{D1}$, $\tilde{B}_{D1}$ etc are constants, and $\tilde{E}_{D1}$ and $\tilde{E}_{D2}$ are decaying exponential terms. The solutions for $D^2(t)$, $\sigma_1^2(t)$ and $\sigma_2^2(t)$ can be calculated from (78), (80) and (81). As with the sinusoidal model, $D_1^2(t) \: t^2$ and $D_2^2(t) \: t$ for the same reasons as discussed previously in Sec. 6.4.

In principle it is possible to calculate general equations for the coefficients in the final solutions that are dependent on λ, d_τ and κ. However, these are long and cumbersome — it is much simpler to solve numerically the systems of equations in (113)-(116) in Appendix B.1 for particular values of the parameters. Numerical values of the coefficients in the final solutions are shown in Appendix B.2 for values of the reorientation parameters that correspond to data set C4 (linear reorientation due to phototaxis) from Hill & Häder (1997), given in Table 1.

8. Simulation results

To test the validity of the asymptotic solutions in Sec. 6.4 and Sec. 7.3, a computer algorithm has been programmed to simulate a population of random walkers moving as a velocity jump process with either the sinusoidal or linear reorientation kernels, and to then calculate the spatial statistics. At each turning step an algorithm from Fisher & Best (1979) is used to simulate the von Mises distribution, and we have also used algorithms RAN1, GAMDEV and BESSI from Press et al. (1992). For full details of the simulation algorithm see Codling (2003). In all the following simulations we assume that the population are moving in the (x, y) plane and the preferred direction is the y-direction (i.e. $x_1 = y$).

8.1. Simulations using experimentally observed parameter values

Comparisons between simulations and the asymptotic solutions have been completed for a large range of parameter values in Codling (2003). Here we present results of simulations for parameter values calculated from the experimental results of Hill & Häder (1997) given in Table 1. Henceforth, from Table 1, we refer to the parameter values calculated using estimates over all sampling times as data sets C1:a and C4:a, and parameter values calculated using the estimates over sampling times $\tau_s < 0.4$ s as data sets C1:b and C4:b.

Simulations of 500 walkers were completed using the sinusoidal reorientation model with reorientation parameters C1:a and C1:b from Table 1, with $\lambda = 1/\tau = 12.5$ s^{-1} and a fixed speed of $s = \bar{s} = 55$ μms^{-1}, taken from the results of Hill & Häder (1997). Similarly, simulations have also been run for data sets C4:a and C4:b from Table 1 using the linear reorientation

model with $\lambda = 1/\tau = 12.5$ s^{-1} and a fixed speed of $s = \bar{s} = 59$ μms^{-1}, again taken from the results of Hill & Häder (1997).

Fig. 1 shows the spatial distribution of the population of walkers at $t = 100$ for the four data sets. It is clear that the different data sets produce a slightly different spatial distribution after a fixed time. It is immediately noticeable that data sets C1:a and C4:a produce a larger spread, while the linear reorientation model (C4:a and C4:b) appears to produce a much larger average drift in the preferred direction. This latter result is confirmed in Fig. 2, that shows the mean position in the preferred direction for the four data sets, $\mathbf{H}_y(t)$ (the average position in the non-preferred direction, $\mathbf{H}_x(t)$, is zero). This can be explained by recalling (14) and (15), where it is clear that the linear reorientation model will always produce a larger reorientation back to the preferred direction at each turning event. There is a very good match between all the asymptotic solutions and the simulation results, while the mean position is quantitatively similar when comparing C1:a with C1:b, and C4:a with C4:b.

Fig. 3 compares the spread about the mean position in each direction, $\sigma_x^2(t)$ and $\sigma_y^2(t)$, for all four data sets. Again, there is a very good match between the asymptotic solutions and the simulation results. As observed in Fig. 1, it is clear that data sets C1:a and C4:a produce a larger spread than C1:b and C4:b respectively. It is also interesting to note that, in data sets C1:a and C1:b, $\sigma_x^2(t) \approx \sigma_y^2(t)$, but in data sets C4:a and C4:b, $\sigma_x^2(t) > \sigma_y^2(t)$. In general, as the random walk becomes more like a straight line in the preferred direction (y), the spread about the mean position will be less in the preferred direction than in the non-preferred direction (x). This effect is explained in Sec. 8.2 and in more detail in Codling (2003), and the effect can be seen in Fig. 1.

8.2. The effect of the reorientation parameters on the approximate steady-state solutions

We have seen that our asymptotic solutions are a very good match to simulated results for parameter values that are observed experimentally. It is also useful to study the effect of a range of values of the reorientation parameters on the approximate steady-state solutions for the spatial statistics. The following simulations have been completed for non-dimensionalised velocity jump processes where we have used $\lambda = \tau = s = 1$, and we have considered the spatial statistics at $t = 100$, the approximate steady-state solutions.

Fig. 4 shows plots of the theoretical asymptotic solution and simulated results for the mean position in the preferred direction at $t = 100$, $\mathbf{H}_y(100)$, for both the sinusoidal and linear reorientation models. For both reorientation models, $\mathbf{H}_y(100)$, increases as the parameter κ increases, although the rate of increase also slows down as κ increases. As $\kappa \to \infty$, $\mathbf{H}_y(100)$ tends asymptotically to the maximum possible displacement, $\mathbf{H}_y(100) = st = 100$, which corresponds to movement in a straight line in the preferred direction.

The average position is larger for larger values of d_τ, and the linear reorientation model produces a larger average position than the sinusoidal model for the same reorientation parameters. There is a very good match between the theoretical asymptotic solutions and the simulation results, both qualitatively and quantitatively. However, if larger values of d_τ are used, and the random walk is no longer approximately smooth, then the asymptotic solutions start to break down.

Fig. 5 shows plots of the theoretical asymptotic solution and simulated results for the spread about the mean position in the non-preferred direction at $t = 100$, $\sigma_x^2(100)$, for both the sinusoidal and linear reorientation models. The simulated results are quite noisy but there is a good qualitative match with the asymptotic solutions.

If there is no bias and $d_\tau = 0$ then the spread increases as κ increases. In this case the mean position will always be the origin as there is no preferred direction, and as $\kappa \to \infty$ the motion of the population will become more like a wave spreading out from the origin and $\sigma_x^2(100)$ will tend asymptotically to the maximum possible value, $s^2 t^2/2 = 5000$.

If bias is present then this is no longer true — in this case $\sigma_x(100)$ initially increases as κ increases and then reaches a maximum value before starting to decrease. In general, $\sigma_x(100)$ is less if d_τ is larger. Consider a random walk where $d_\tau \neq 0$ and $\kappa \to \infty$: as long as there is some bias present then by increasing κ the motion of the population becomes more like a straight line in the preferred direction rather than a wave spreading out from a central point. As $\kappa \to \infty$, the walkers will tend to have a mean position of $\mathbf{H}(100) \approx (0, 100)$, and thus $D_x^2(100) \to 0$, $D_y^2 \to 10\,000$ and $\sigma_x^2 \to 0$. For the same parameter values, the linear model has less spread in the non-preferred direction than the sinusoidal model.

Fig. 6 shows similar results: if $d_\tau = 0$ then $\sigma_y^2(100)$ increases asymptotically as κ increases, up to the maximum possible value of $s^2 t^2/2 = 5000$, while if there is bias and $d_\tau \neq 0$ then $\sigma_y^2(100)$ reaches a maximum value and then starts to decrease as κ increases, for the same reasons as described previously. For small values of the reorientation parameters there is a good qualitative match between the asymptotic solutions and the simulated results, but at large values the theoretical model clearly breaks down as it is not possible to have 'negative spread'. As was the case previously, $\sigma_y^2(100)$ is smaller if d_τ is larger, and smaller for the linear reorientation model when compared to the sinusoidal model for the same parameter values.

Simulations have been used to investigate larger parameter values where the underlying random walk is no longer approximately smooth and the asymptotic solutions break down (Codling, 2003), but these parameter values are not realistic to describe the motion of swimming micro-organisms using a continuously turning random walk model and results are not presented in this paper.

9. Discussion

We have presented a new application of the velocity jump process model introduced by Othmer et al. (1988) that describes the motion of swimming micro-organisms and other animals or cells that move with a directed motion. The velocity jump model is more realistic than simple diffusion models as the speed of movement is fixed, but it is not possible to derive an equation for the underlying spatial distribution of such a process directly (Hillen, 2002). Our random walk model includes the sinusoidal and linear reorientation models observed by Hill & Häder (1997) in experiments on swimming algae. In contrast to the particular case of the 'random walk in external field' in Othmer et al. (1988), our reorientation kernel, $T(\theta, \theta')$ includes the effects of bias and correlation in one probability distribution that has two parameters κ and d_τ, and we do not need to make a superposition of two separate distributions.

The reorientation parameters, κ and d_τ, can be measured directly from simple experimental observations (Hill & Häder, 1997; Codling & Hill, 2004). Using a transport equation (see Hillen, 2002; Hillen & Othmer, 2000; Othmer & Hillen, 2002) and various moment closure assumptions we have derived and solved a system of differential equations for the spatial statistics and higher moments. These asymptotic solutions are a very good match to simulated random walks for realistic parameter values.

As discussed in Sec. 3.1, our choice of $\mu_\delta(\theta')$ in the reorientation kernel, $T(\theta, \theta')$, violates assumption T4, (8), in the general theory of velocity jump processes given in, for example, Hillen & Othmer (2000) and Hillen (2002). Thus, many of their general results may not be applicable to our model. The reorientation models in (14) and (15) from Hill & Häder (1997), implicitly assume that the preferred direction is fixed and bias is spatially independent and only introduced through the dependence of the mean turning angle on the previous direction of movement. This assumption is reasonable if movement is due to, for example gyrotaxis (Kessler, 1986) or phototaxis where the distance to the light source is large compared to the scale of movement (Hill & Vincent, 1993). However, (14) and (15) are not appropriate if the preferred direction is likely to change (e.g. random walkers moving towards a point source), or if the level of the introduced bias changes with spatial position (e.g. walkers moving up a chemical gradient). In Codling et al. (2004), we simulate reef fish larvae orientating back to a circular reef by adapting (14) and (15) to allow for a changing preferred direction, and allowing κ and d_τ to be spatially dependent, but in this example the asymptotic solutions in Sec. 6.4 and Sec. 7.3 are not valid.

We have presented a new approach to modelling the directed movement of animals and micro-organisms using a velocity jump process where bias is introduced through the dependence of the mean turning angle on the absolute angle with the sinusoidal or linear reorientation models. Using a combination of asymptotic results, experimental observation and simula-

tions, similar models can be used to model many biological systems where there is a similar directed motion.

APPENDICES

A. Sinusoidal reorientation model

A.1. System of differential equations

Using the same method as in Sec. 6.3 we arrive at the following leading order system of differential equations for the higher moments of the spatial distribution:

$$\frac{d\mathbf{H}}{dt} = \mathbf{V} = s(F_1, Y_1), \tag{82}$$

$$\begin{pmatrix} \dot{F}_1 \\ \dot{F}_2 \end{pmatrix} = \begin{pmatrix} -\lambda_{11} & -\hat{a}_1 \\ \hat{b}_1 & -\lambda_2 \end{pmatrix} \begin{pmatrix} F_1 \\ F_2 \end{pmatrix} + \begin{pmatrix} \hat{a}_2 A_3(w) \\ -\hat{b}_1 A_3(w) + \hat{b}_2(1 + A_4(w)) \end{pmatrix}, \tag{83}$$

$$\begin{pmatrix} \dot{Y}_1 \\ \dot{Y}_2 \end{pmatrix} = \begin{pmatrix} -\lambda_{12} & -\hat{a}_1 \\ \hat{b}_1 & -\lambda_2 \end{pmatrix} \begin{pmatrix} Y_1 \\ Y_2 \end{pmatrix}, \tag{84}$$

$$\frac{dD_1^2}{dt} = 2sG_1, \qquad \frac{dD_2^2}{dt} = 2sZ_1, \tag{85}$$

$$\begin{pmatrix} \dot{G}_1 \\ \dot{G}_2 \end{pmatrix} = \frac{s}{2} \begin{pmatrix} 1 + F_2 \\ F_1 + A_3(w) \end{pmatrix} + \begin{pmatrix} -\lambda_{11} & -\hat{a}_1 \\ \hat{b}_1 & -\lambda_2 \end{pmatrix} \begin{pmatrix} G_1 \\ G_2 \end{pmatrix}$$
$$+ \begin{pmatrix} \hat{a}_2 A_3(w) \\ -\hat{b}_1 A_3(w) + \hat{b}_2(1 + A_4(w)) \end{pmatrix} \bar{x}_1, \tag{86}$$

and

$$\begin{pmatrix} \dot{Z}_1 \\ \dot{Z}_2 \end{pmatrix} = \frac{s}{2} \begin{pmatrix} 1 - F_2 \\ F_1 - A_3(w) \end{pmatrix} + \begin{pmatrix} -\lambda_{12} & -\hat{a}_1 \\ \hat{b}_1 & -\lambda_2 \end{pmatrix} \begin{pmatrix} Z_1 \\ Z_2 \end{pmatrix}, \tag{87}$$

where

$$\lambda_2 = \lambda \left(1 - (1 - d_\tau^2) A_2(\kappa) \right), \quad \lambda_{12} = \lambda \left(1 - (1 - 3d_\tau^2/8) A_1(\kappa) \right),$$
$$\hat{b}_1 = \lambda d_\tau A_2(\kappa), \quad \hat{b}_2 = \lambda d_\tau^2 A_2(\kappa)/2, \tag{88}$$

and $\hat{a}_1$ and $\hat{a}_2$ are as defined in (46).

Note that, due to the way the differential equations are derived, (82) and (85) are the same for all reorientation kernels, $T(\theta, \theta')$. These differential equations are the same for both our sinusoidal and linear reorientation models, and are the same as differential equations (74) and (76) in Othmer et al. (1988) which were derived for a different reorientation model.

This is because, when deriving these equations using the method described in Sec. 6.3, the term in the transport equation (1) that includes the reorientation kernel $T(\theta, \theta')$ is not multiplied by a term dependent on θ. The integral term then takes the form

$$\int_{R^2} \int_{-\pi}^{\pi} \int_{-\pi}^{\pi} T(\theta, \theta') p(\mathbf{x}, \theta', t) d\theta' d\theta \ d\mathbf{x} = N_0, \tag{89}$$

and thus the differential equation derived is always the same as long as the reorientation kernel used is only dependent on the direction of movement. Further details of how the differential equations are derived are given in Codling (2003).

A.2. Solutions

As the differential equations given in Appendix A.1 are all linear with constant coefficients they are straightforward to solve; see Codling (2003) for full details.

The solutions for $\mathbf{V}(t)$ and $\mathbf{H}(t)$ are given in (47) and (48) in the main text and the coefficients in the solutions are defined in Appendix A.3.

The solutions for the spread about the origin in each direction, $D_1^2(t)$ and $D_2^2(t)$, are

$$
\begin{aligned}
D_1^2(t) = 2s^2 \Bigg(& \frac{(A_{f1} + B_{f1})^2}{2} t^2 + A_{g1} \left(t - \frac{1}{\phi_1}(1 - e^{-\phi_1 t}) \right) \\
& + B_{g1} \left(t - \frac{1}{\phi_2}(1 - e^{-\phi_2 t}) \right) - \frac{C_{g1}}{\phi_1} \left(t e^{-\phi_1 t} - \frac{1}{\phi_1}(1 - e^{-\phi_1 t}) \right) \\
& - \frac{D_{g1}}{\phi_2} \left(t e^{-\phi_2 t} - \frac{1}{\phi_2}(1 - e^{-\phi_2 t}) \right) \\
& + E_{g1} \left(\frac{1}{\phi_1}(1 - e^{-\phi_1 t}) - \frac{1}{\phi_2}(1 - e^{-\phi_2 t}) \right) \Bigg),
\end{aligned} \tag{90}
$$

and

$$
\begin{aligned}
D_2^2(t) = 2s^2 \Bigg(& (A_{z1} + B_{z1}) t - \frac{1}{\phi_3}(A_{z1} + C_{z1} + D_{z1}) \left(1 - e^{-\phi_3 t} \right) \\
& - \frac{1}{\phi_4}(B_{z1} + E_{z1} + F_{z1}) \left(1 - e^{-\phi_4 t} \right) + \frac{1}{\phi_1}(C_{z1} + E_{z1}) \left(1 - e^{-\phi_1 t} \right) \\
& + \frac{1}{\phi_2}(D_{z1} + F_{z1}) \left(1 - e^{-\phi_2 t} \right) \Bigg),
\end{aligned} \tag{91}
$$

where the coefficients in the solutions are defined in Appendix A.3.

A.3. Coefficients in the final solutions

The solutions given in Sec. 6.4 have been left in a general form. The coefficients in (47) and (48) are defined as follows:

$$\phi_1 = \frac{1}{2}\left(\lambda_{11} + \lambda_2 - \sqrt{(\lambda_{11} - \lambda_2)^2 - 4\hat{a}_1\hat{b}_1}\right), \tag{92}$$

$$\phi_2 = \frac{1}{2}\left(\lambda_{11} + \lambda_2 + \sqrt{(\lambda_{11} - \lambda_2)^2 - 4\hat{a}_1\hat{b}_1}\right), \tag{93}$$

$$A_{f1} = \frac{\lambda_2 - \phi_1}{\hat{b}_1\phi_1(\phi_2 - \phi_1)}\left(\hat{b}_1 C_{f1} - (\lambda_2 - \phi_2)C_{f2}\right), \tag{94}$$

$$B_{f1} = \frac{-(\lambda_2 - \phi_2)}{\hat{b}_1\phi_2(\phi_2 - \phi_1)}\left(\hat{b}_1 C_{f1} - (\lambda_2 - \phi_1)C_{f2}\right), \tag{95}$$

$$A_{f2} = \frac{1}{\phi_1(\phi_2 - \phi_1)}\left(\hat{b}_{s1} C_{f1} - (\lambda_2 - \phi_2)C_{f2}\right), \tag{96}$$

$$B_{f2} = \frac{-1}{\phi_2(\phi_2 - \phi_1)}\left(\hat{b}_{s1} C_{f1} - (\lambda_2 - \phi_1)C_{f2}\right), \tag{97}$$

where the terms C_{f1} and C_{f2} correspond to the constant terms in the systems of differential equations (83) and (86) and are given by

$$C_{f1} = (\hat{a}_1 + \hat{a}_2 A_3(w)) \tag{98}$$

$$C_{f2} = \left(\hat{b}_2(1 + A_4(w)) - \hat{b}_1 A_3(w)\right) \tag{99}$$

and all other constant terms are as defined in (46) or (88).

The coefficients in (90) and (91) are defined as follows:

$$A_{g1} = -\frac{2A_{f1}^2}{\phi_1} - A_{f1}B_{f1}\left(\frac{1}{\phi_1} + \frac{1}{\phi_2}\right) + \frac{(\lambda_2 - \phi_1)}{2\phi_1(\phi_2 - \phi_1)}(1 + A_{f2} + B_{f2})$$
$$- \frac{(\lambda_2 - \phi_1)(\lambda_2 - \phi_2)}{2\hat{b}_{s1}\phi_1(\phi_2 - \phi_1)}(A_{f1} + B_{f1} + A_3(z)), \tag{100}$$

$$B_{g1} = -\frac{2B_{f1}^2}{\phi_2} - A_{f1}B_{f1}\left(\frac{1}{\phi_1} + \frac{1}{\phi_2}\right) - \frac{(\lambda_2 - \phi_2)}{2\phi_2(\phi_2 - \phi_1)}(1 + A_{f2} + B_{f2})$$
$$+ \frac{(\lambda_2 - \phi_1)(\lambda_2 - \phi_2)}{2\hat{b}_{s1}\phi_2(\phi_2 - \phi_1)}(A_{f1} + B_{f1} + A_3(z)), \tag{101}$$

$$C_{g1} = A_{f1}^2 + \frac{(\lambda_2 - \phi_1)}{2\hat{b}_{s1}(\phi_2 - \phi_1)}\left(A_{f1}(\lambda_2 - \phi_2) - A_{f2}\hat{b}_{s1}\right), \tag{102}$$

$$D_{g1} = B_{f1}^2 - \frac{(\lambda_2 - \phi_2)}{2\hat{b}_{s1}(\phi_2 - \phi_1)}\left(B_{f1}(\lambda_2 - \phi_1) - B_{f2}\hat{b}_{s1}\right), \tag{103}$$

$$E_{g1} = -\frac{(\lambda_2 - \phi_1)\left(\hat{b}_{s1}(\phi_2 B_{f2} - 2C_{f1}B_{f1}) - B_{f1}(\lambda_2 - \phi_2)(\phi_2 - 2C_{f2})\right)}{2\phi_2 \hat{b}_{s1}(\phi_2 - \phi_1)^2}$$

$$+ \frac{(\lambda_2 - \phi_2)\left(\hat{b}_{s1}(\phi_1 A_{f2} - 2C_{f1}A_{f1}) - A_{f1}(\lambda_2 - \phi_1)(\phi_1 - 2C_{f2})\right)}{2\phi_1 \hat{b}_{s1}(\phi_2 - \phi_1)^2},$$

$$(104)$$

and

$$\phi_3 = \frac{1}{2}\left(\lambda_{12} + \lambda_2 - \sqrt{(\lambda_{12} - \lambda_2)^2 - 4\hat{a}_{s1}\hat{b}_{s1}}\right), \qquad (105)$$

$$\phi_4 = \frac{1}{2}\left(\lambda_{12} + \lambda_2 + \sqrt{(\lambda_{12} - \lambda_2)^2 - 4\hat{a}_{s1}\hat{b}_{s1}}\right), \qquad (106)$$

$$A_{z1} = \frac{(\lambda_2 - \phi_3)}{2\hat{b}_{s1}\phi_3(\phi_4 - \phi_3)}\Big(\hat{b}_{s1}(1 - A_{f2} - B_{f2})$$

$$-(\lambda_2 - \phi_4)(A_{f1} + B_{f1} - A_3(z))\Big), \qquad (107)$$

$$B_{z1} = -\frac{(\lambda_2 - \phi_4)}{2\hat{b}_{s1}\phi_4(\phi_4 - \phi_3)}\Big(\hat{b}_{s1}(1 - A_{f2} - B_{f2})$$

$$-(\lambda_2 - \phi_3)(A_{f1} + B_{f1} - A_3(z))\Big), \qquad (108)$$

$$C_{z1} = \frac{(\lambda_2 - \phi_3)}{2\hat{b}_{s1}(\phi_3 - \phi_1)(\phi_4 - \phi_3)}\left(\hat{b}_{s1}A_{f2} + (\lambda_2 - \phi_4)A_{f1}\right), \qquad (109)$$

$$D_{z1} = \frac{(\lambda_2 - \phi_3)}{2\hat{b}_{s1}(\phi_3 - \phi_2)(\phi_4 - \phi_3)}\left(\hat{b}_{s1}B_{f2} + (\lambda_2 - \phi_4)B_{f1}\right), \qquad (110)$$

$$E_{z1} = -\frac{(\lambda_2 - \phi_4)}{2\hat{b}_{s1}(\phi_4 - \phi_1)(\phi_4 - \phi_3)}\left(\hat{b}_{s1}A_{f2} + (\lambda_2 - \phi_3)A_{f1}\right), \qquad (111)$$

$$F_{z1} = -\frac{(\lambda_2 - \phi_4)}{2\hat{b}_{s1}(\phi_4 - \phi_2)(\phi_4 - \phi_3)}\left(\hat{b}_{s1}B_{f2} + (\lambda_2 - \phi_3)B_{f1}\right), \qquad (112)$$

where ϕ_1, ϕ_2, A_{f1}, B_{f1}, A_{f2}, and B_{f2} are as defined in (92) — (97), and all other constant terms are as defined in (46) or (88).

B. Linear reorientation model

B.1. System of differential equations

For simplicity, we can write the first system as

$$
\begin{pmatrix} \dot{F_1} \\ \dot{K_1} \\ \dot{M_1} \\ \dot{F_2} \\ \dot{K_2} \\ \dot{M_2} \end{pmatrix} = \mathbf{A} \begin{pmatrix} F_1 \\ K_1 \\ M_1 \\ F_2 \\ K_2 \\ M_2 \end{pmatrix} + \begin{pmatrix} 0 \\ \lambda \\ -2\lambda \\ 0 \\ -\lambda/2 \\ \lambda/2 \end{pmatrix}, \tag{113}
$$

where the coefficients in the matrix $\mathbf{A}$ are dependent on λ, d_τ and κ, and are given below. Similarly, we can write the other system as

$$
\begin{pmatrix} \dot{Y_1} \\ \dot{L_1} \\ \dot{N_1} \\ \dot{Y_2} \\ \dot{L_2} \\ \dot{N_2} \end{pmatrix} = \mathbf{B} \begin{pmatrix} Y_1 \\ L_1 \\ N_1 \\ Y_2 \\ L_2 \\ N_2 \end{pmatrix}, \tag{114}
$$

$$
\begin{pmatrix} \dot{G_1} \\ \dot{P_1} \\ \dot{R_1} \\ \dot{G_2} \\ \dot{P_2} \\ \dot{R_2} \end{pmatrix} = \mathbf{A} \begin{pmatrix} G_1 \\ P_1 \\ R_1 \\ G_2 \\ P_2 \\ R_2 \end{pmatrix} + \begin{pmatrix} 0 \\ \lambda \\ -2\lambda \\ 0 \\ -\lambda/2 \\ \lambda/2 \end{pmatrix} \bar{x}_1 + \frac{s}{2} \begin{pmatrix} 1 + F_2 \\ K_2 \\ M_0 + M_2 \\ F_1 + F_3 \\ K_1 + K_3 \\ M_1 + M_3 \end{pmatrix}, \tag{115}
$$

and

$$
\begin{pmatrix} \dot{Z_1} \\ \dot{Q_1} \\ \dot{S_1} \\ \dot{Z_2} \\ \dot{Q_2} \\ \dot{S_2} \end{pmatrix} = \mathbf{B} \begin{pmatrix} Z_1 \\ Q_1 \\ S_1 \\ Z_2 \\ Q_2 \\ S_2 \end{pmatrix} + \frac{s}{2} \begin{pmatrix} 1 - F_2 \\ K_2 \\ M_0 - M_2 \\ F_1 - F_3 \\ K_3 - K_1 \\ M_1 - M_3 \end{pmatrix}, \tag{116}
$$

where the coefficients in the matrix $\mathbf{B}$ are also dependent on λ, d_τ and κ, and are given below, and the moments M_0, F_3, K_3 and M_3 are approximated using the expected long-time angular distribution equation, (17), from Hill & Häder (1997) in place of $f(\theta)$ (closure assumption 2 in Sec. 7.2).

The matrices in (113), (115) and (116) are

$\mathbf{A} \;=\;$

$$-\lambda \begin{pmatrix} 1-A_1 & -d_\tau A_1 & \frac{1}{2}d_\tau^2 A_1 & 0 & 0 & 0 \\ \frac{1}{2}A_1 & 1+\frac{1}{2}d_\tau A_1 & -\frac{1}{4}d_\tau^2 A_1 & \frac{1}{2}A_2 & d_\tau A_2 & -d_\tau^2 A_2 \\ -4A_1 & -4d_\tau A_1 & 1+2d_\tau^2 A_1 & 2A_2 & 4d_\tau A_2 & -4d_\tau^2 A_2 \\ 0 & 0 & 0 & 1-A_2 & -2d_\tau A_2 & 2d_\tau^2 A_2 \\ -\frac{3}{2}A_1 & -\frac{3}{2}d_\tau A_1 & \frac{3}{4}d_\tau^2 A_1 & \frac{3}{4}A_2 & 1+\frac{3}{2}d_\tau A_2 & -\frac{3}{2}d_\tau^2 A_2 \\ 2A_1 & 2d_\tau A_1 & -d_\tau^2 A_1 & -3A_2 & -6d_\tau A_2 & 1+6d_\tau^2 A_2 \end{pmatrix},$$

(117)

and

$$\mathbf{B} = $$
$$-\lambda \begin{pmatrix} 1-A_1 & d_\tau A_1 & \frac{1}{2}d_\tau^2 A_1 & 0 & 0 & 0 \\ \frac{1}{2}A_1 & 1-\frac{1}{2}d_\tau A_1 & -\frac{1}{4}d_\tau^2 A_1 & -A_2 & 2d_\tau A_2 & 2d_\tau^2 A_2 \\ -3A_1 & 3d_\tau A_1 & 1+\frac{3}{2}d_\tau^2 A_1 & 0 & 0 & 0 \\ 0 & 0 & 0 & 1-A_2 & 2d_\tau A_2 & 2d_\tau^2 A_2 \\ \frac{3}{4}A_1 & -\frac{3}{4}d_\tau A_1 & -\frac{3}{8}d_\tau^2 A_1 & A_2 & 1-d_\tau A_2 & -d_\tau^2 A_2 \\ 2A_1 & -2d_\tau A_1 & -d_\tau^2 A_1 & -4A_2 & 8d_\tau A_2 & 1+8d_\tau^2 A_2 \end{pmatrix},$$

(118)

where $A_n = I_n(\kappa)/I_0(\kappa)$.

B.2. Numerical coefficients in the asymptotic solutions

The solutions in Sec. 7.3 have the following values for the coefficients when the parameters for data sets corresponding to linear reorientation due to phototaxis (C4:a and C4:b from Table 1) are used, and $\bar{\tau} = 0.08$ s (all solutions are rounded to two decimal places):

C4:a

$$\mathbf{H}_y(t) = 22.07t - 42.77 + 43.23e^{-0.53t} - 0.35e^{-1.73t}, \tag{119}$$
$$\sigma_x^2(t) = 9644.20t - 24065.69 + 9738.34e^{-0.53t} - 177.78e^{-1.73t}$$
$$+ 14818.34e^{-0.35t} - 313.32e^{-1.31t} + 0.01e^{-12.50t}, \tag{120}$$
$$\sigma_y^2(t) = 4800.97t - 4853.70 - 2983.67te^{-0.53t} + 23.56te^{-1.73t}$$
$$+ 6504.55e^{-0.53t} + 178.77e^{-1.73t} - 1859.88e^{-1.05t} + 30.39e^{-2.25t}$$
$$- 0.12e^{-3.45t} - 0.02e^{-12.50t}. \tag{121}$$

C4:b

$$\mathbf{H}_y(t) = 20.81t - 12.07 + 12.18e^{-1.75t} - 0.11e^{-5.07t}, \tag{122}$$
$$\sigma_x^2(t) = 2807.70t - 2069.59 + 837.38e^{-1.75t} - 16.92e^{-5.07t} + 1281.15e^{-1.21t}$$

$$-31.89e^{-4.07t} - 0.14e^{-12.50t}, \tag{123}$$

$$\sigma_y^2(t) = 1494.26t - 497.07 - 812.38te^{-1.75t} + 7.95te^{-5.07t} + 623.21e^{-1.75t}$$
$$+19.68e^{-5.07t} - 148.46e^{-3.51t} + 2.73e^{-6.83t} - 0.01e^{-10.15t}$$
$$-0.07e^{-12.50t}. \tag{124}$$

References

Batschelet, E.: *Circular Statistics in Biology*. Academic Press, London, 1981.

Bovet, P., Benhamou, S.: Spatial analysis of animals' movements using a correlated random walk model. J., Theo. Biol. **131,** 419-433 (1988).

Codling, E.A.: *Biased Random Walks in Biology* PhD Thesis. Leeds University, 2003. http://www.maths.leeds.ac.uk/Applied/phd/codling.html

Codling, E.A., Hill, N.A.: Sampling rate effects on measurements of correlated and biased random walks. Submitted to J. Theor. Biol. (2004).

Codling, E.A., Hill, N.A., Pitchford, J.W., Simpson, S.: Random walk models for the movement and recruitment of reef fish larvae. Mar. Ecol. Prog. Ser. (2004), in press.

Dolak, Y., Hillen, T.: Cattaneo models of chemosensitive movement: numerical solution and pattern formation. J. Math. Biol. **46,** 153-170 (2003).

Fisher, N.I., Best, D.J.: Efficient simulation of the von Mises distribution. Appl. Stat. **28,** 152-157 (1979).

Ford, R.M., Lauffenburger, D.A.: Measurement of bacterial random motility and chemotaxis coefficients: II. application of single cell based mathematical model. Biotechnol. Bioeng. **37,** 661-672 (1991).

Ghovai, S., Hill, N.A.: Penetrative phototactic bioconvection. Submitted to Phys. Fluids (2004).

Goldstein, S.: On diffusion by discontinuous movements, and on the telegraph equation. J. Mech. App. Math. **6,** 129-156 (1951).

Hill, N.A., Häder, D.P.: A biased random walk model for the trajectories of swimming micro-organisms. J. Theo. Biol. **186,** 503-526 (1997).

Hill, N.A., Vincent, R.V.: A simple model and strategies for orientation in phototactic micro-organisms. J. Theo. Biol. **163,** 223-235 (1993).

Hillen, T.: Hyperbolic models for chemosensitive movement. Math. Mod. Meth. in Appl. Sci. **12,** 1007-1034 (2002).

Othmer, H.G., Hillen, T.: The diffusion limit of transport equations derived from velocity jump processes. S.I.A.M. J. Appl. Math. **61,** 751-775 (2000).

Kac, M.: A stochastic model related to the telegraphers equation. Rocky Mtn. J. Maths. **4,** 497-509 (1974).

Kareiva, P.M., Shigesada, N.: Analyzing insect movement as a correlated random walk. Oecologia **56,** 234-238 (1983).

Kessler, J.O.: Individual and collective fluid dynamics of swimming cells. J. Fluid Mech. **73,** 191-205 (1986).

Mardia, K.V., Jupp, P.E.: *Directional Statistics*. Wiley, Chichester, 1999.

Okubo, A.: *Diffusion and Ecological Problems: Mathematical Models*. Springer-Verlag, Berlin, 1980.

Othmer, H.G., Dunbar, S.R., Alt, W.: Models of dispersal in biological systems. J. Math. Biol. **26,** 263-298 (1988).

Othmer, H.G., Hillen, T.: The diffusion limit of transport equations II: Chemotaxis equations. S.I.A.M. J. Appl. Math. **62,** 1222-1250 (2002).

Press, W.H. et al. *Numerical Recipes in C: The Art of Scientific Computing* (Cambridge University Press, Cambridge 1992).

Siniff, D.P., Jessen, C.R.: A simulation model of animal movement patterns. Adv. Ecol. Res. **6,** 185-219 (1969).

(a) C1:a at $t = 100$

(b) C1:b at $t = 100$

(c) C4:a at $t = 100$

(d) C4:b at $t = 100$
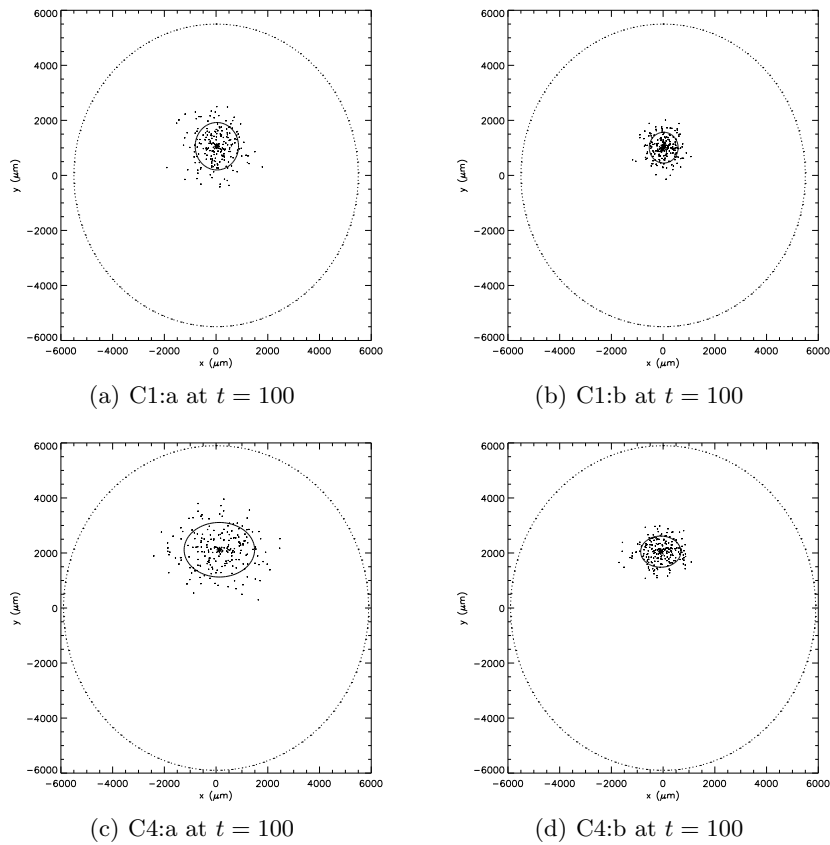
Fig. 1. Plots showing simulated position and spread at $t = 100$ for parameters calculated from data set (a) C1:a; (b) C1:b; (c) C4:a; and (d) C4:b. The actual parameter values used are given in Table 1. Legend: (—) population spread about the mean position, $\sqrt{\sigma^2(100)}$, ($\cdots$) theoretical maximum displacement, st; individual positions are marked by points.

(a) $\mathbf{H}_y(t)$ for C1   (b) $\mathbf{H}_y(t)$ for C4
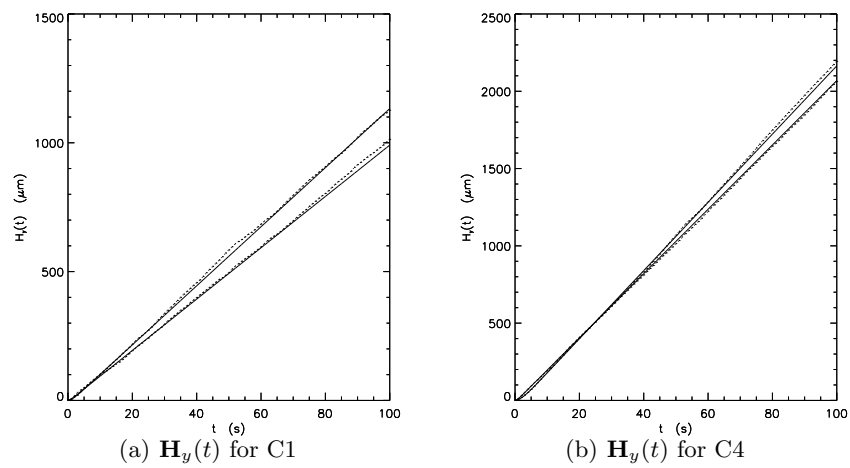
Fig. 2. Plots showing (a) $\mathbf{H}_y(t)$ for parameter values calculated from data set C1:a and C1:b, and (b) $\mathbf{H}_y(t)$ for C4:a and C4:b. The actual parameter values used are given in Table 1. Legend: (—) asymptotic solution, ($\cdots$) simulated results. In (a) C1:a, and in (b) C4:a, are the plots with the largest value of $\mathbf{H}_y(100)$. Note that the scale of each plot is different.

(a) $\sigma_x^2(t)$ for C1

(b) $\sigma_y^2(t)$ for C1

(c) $\sigma_x^2(t)$ for C4
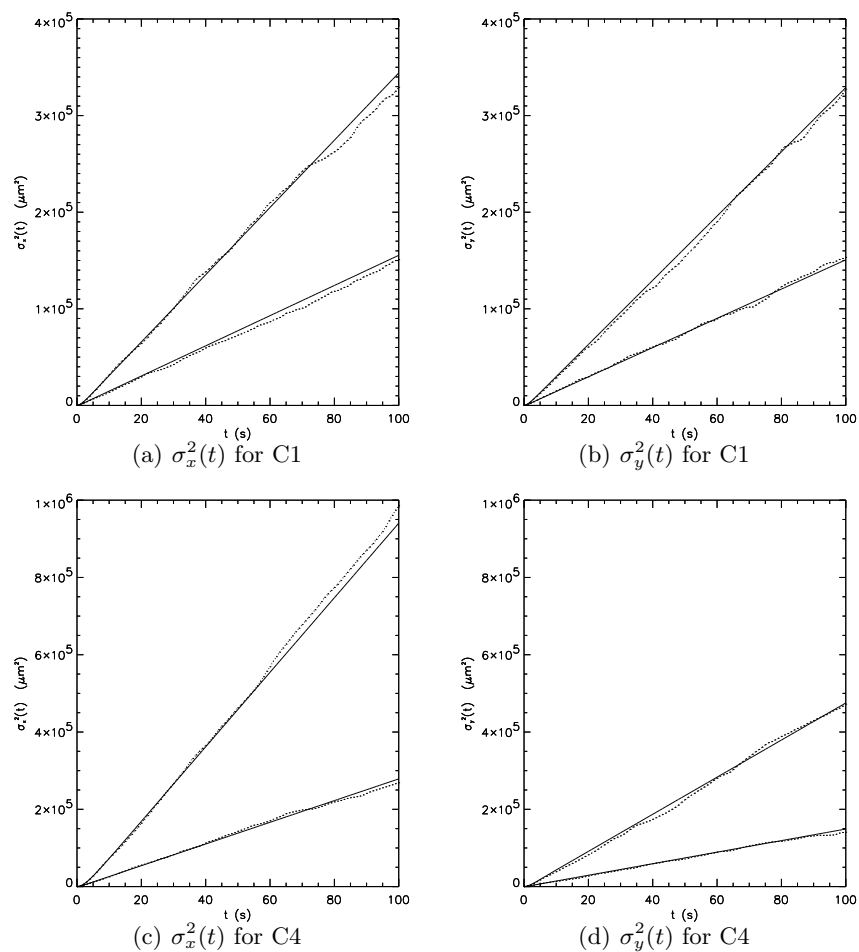
(d) $\sigma_y^2(t)$ for C4

Fig. 3. Plots showing (a) $\sigma_x^2(t)$ for C1:a and C1:b; (b) $\sigma_y^2(t)$ for C1:a and C1:b, (c) $\sigma_x^2(t)$ for C4:a and C4:b; and (d) $\sigma_y^2(t)$ for C4:a and C4:b. In (a) and (b), $\sigma_x^2(t)$ and $\sigma_y^2(t)$ are always larger for data set C1:a; in (c) and (d), $\sigma_x^2(t)$ and $\sigma_y^2(t)$ are always larger for data set C4:a. Legend: (—) asymptotic solution, ($\cdots$) simulated results.
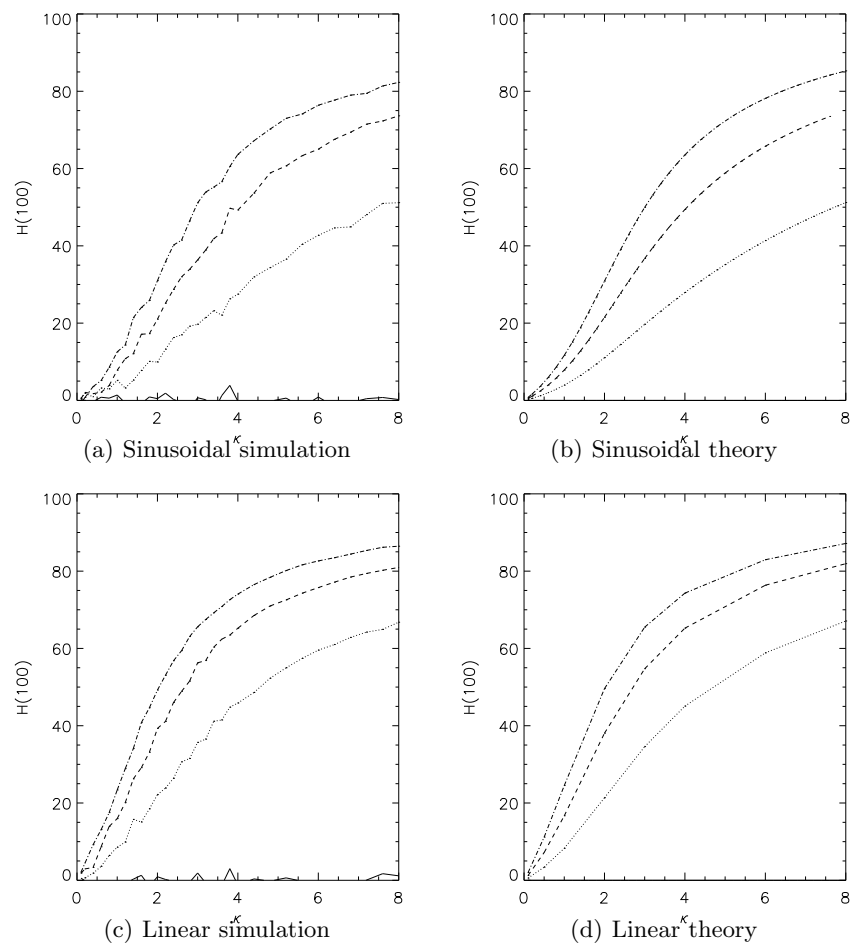
Fig. 4. Plots showing $\mathbf{H}_y(100)$ against κ for sinusoidal and linear reorientation with $d_\tau = 0$ (—), $d_\tau = 0.1$ ($\cdots$), $d_\tau = 0.2$ (−−) and $d_\tau = 0.3$ ($\cdot - \cdot$).
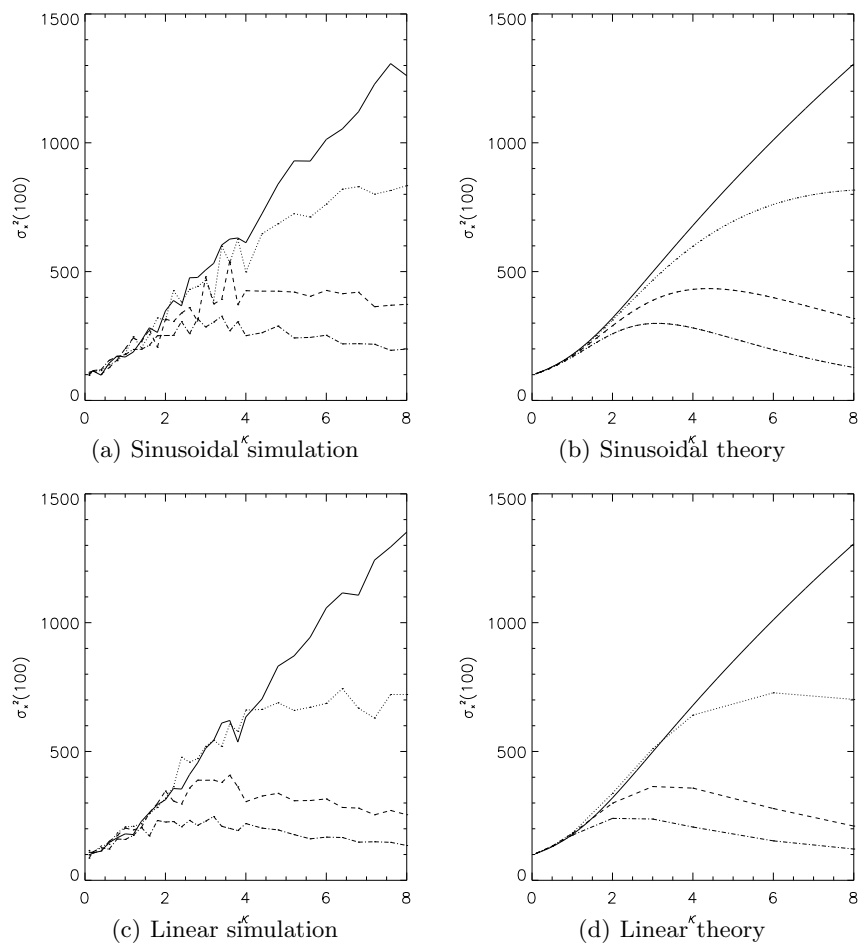
Fig. 5. Plots showing $\sigma_x^2(100)$ against κ for sinusoidal and linear reorientation with $d_\tau = 0$ (—), $d_\tau = 0.1$ ($\cdots$), $d_\tau = 0.2$ ($--$) and $d_\tau = 0.3$ ($\cdot - \cdot$).
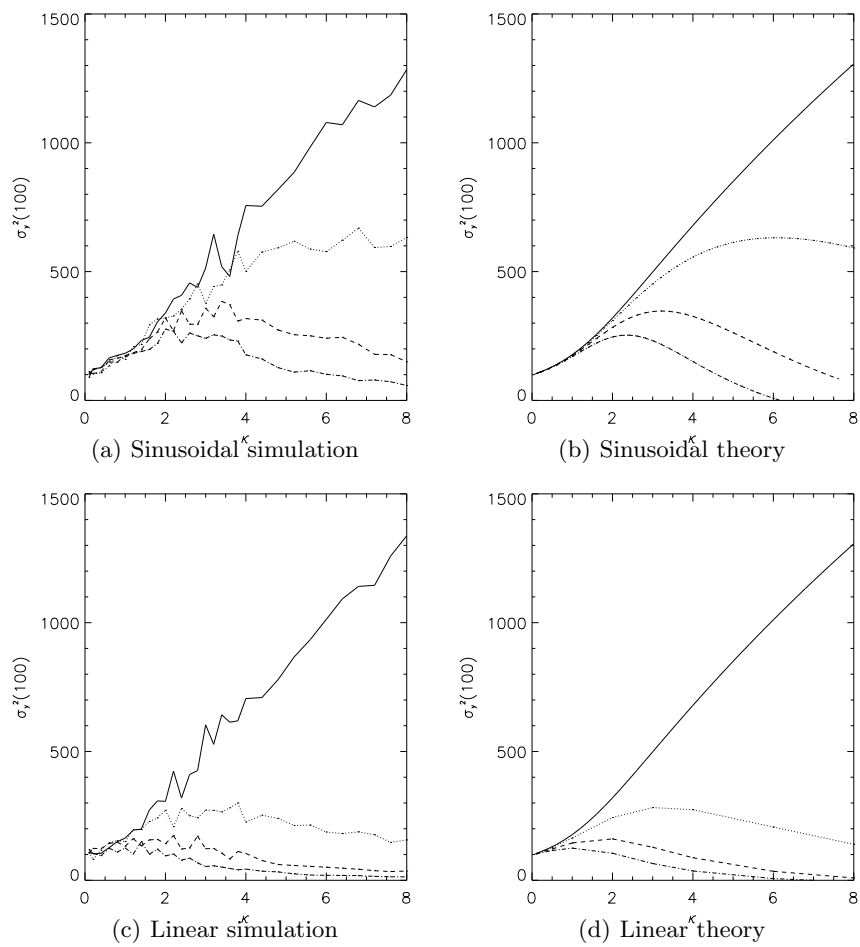
Fig. 6. Plots showing $\sigma_y^2(100)$ against κ for sinusoidal and linear reorientation with $d_\tau = 0$ (—), $d_\tau = 0.1$ ($\cdots$), $d_\tau = 0.2$ ($--$) and $d_\tau = 0.3$ ($\cdot - \cdot$). Note that in (d) the theoretical asymptotic solutions break down as they predict 'negative spread'.